

# Asymmetricity and sign reversal of secondary Bjerknes force from strong nonlinear coupling in cavitation bubble pairs <sup>a</sup>

Vikash Pandey\*

*Centre for Ecological and Evolutionary Synthesis (CEES),*

*Department of Biosciences, University of Oslo,*

*P.O. Box 1066, NO-0316, Oslo, NORWAY<sup>b</sup>*

*Research Centre for Arctic Petroleum Exploration (ARCEX),*

*Department of Geosciences, UiT The Arctic University of Norway in Tromsø,*

*P.O. Box 6050, N-9037, Tromsø, NORWAY*

(Dated: December 15, 2024)

## Abstract

Most of the current applications of acoustic cavitation use bubble-clusters that exhibit multi-bubble dynamics. This necessitates a complete understanding of the mutual nonlinear coupling between individual bubbles. In this study, strong nonlinear coupling is investigated in bubble-pairs which is the simplest case of a bubble-cluster. This leads to the derivation of a more comprehensive set of coupled Keller-Miksis equations (KMEs) that contain nonlinear coupling terms of higher order. The governing KMEs take into account the convective contribution that stems from the Navier-Stokes equation. The system of KMEs is numerically solved for acoustically excited bubble pairs. It is shown that the higher order corrections are important in the estimation of secondary Bjerknes force for closely-spaced bubbles. Further, asymmetricity is witnessed in both magnitude and sign reversal of the secondary Bjerknes force in weak, regular, and strong acoustic fields. The obtained results are examined in the light of published scientific literature. It is expected that the findings reported in this paper may have implications in industries where there is a requirement to have a control on cavitation and its effects.

## PACS numbers:

PACS numbers: 47.55.dd, 43.35.Ei, 47.55.Bx, 43.30.Nb, 43.25.Ts, 47.61.Jd, 43.25.Yw, 43.25.+y

---

<sup>a</sup> [Revised preprint submitted to the Physical Review E](#)

<sup>b</sup> Current affiliation.

\* vikashp@ifi.uio.no

## I. INTRODUCTION

Acoustic cavitation is defined as the formation and pulsation of gas cavities in a liquid under the action of an acoustic field [1, 2]. The cavities often grow as microbubbles and exhibit a cache of exotic phenomena in their relatively short life-time. This may include; rapid oscillations, high speed liquid micro-jets, emanation of capillary waves and shock waves, and finally a violent collapse with sonoluminescence [3–5]. The motivation to study cavitation bubbles has changed in the last one century from scientific curiosity [6] to application driven [2, 7–11]. In most applications, bubble-clusters are manipulated by irradiating them with an acoustic wave. Bubbles first experience a primary Bjerknes force due to the direct impact from the incident wave. Consequently, bubbles may translate toward the pressure antinode if their equilibrium radii is smaller than the resonance size corresponding to the wave frequency. Otherwise, the bubbles migrate toward the pressure node.

But, this study focuses on the secondary Bjerknes force that oscillating bubbles exert on each other through the re-radiation of the acoustic field [12]. This is because even though the primary Bjerknes force is usually stronger than the secondary Bjerknes force for bubbles separated by large distances, the former can be successfully circumvented through clever designing of the experimental apparatus [12, 13]. Besides, the origin and implications of the primary Bjerknes force are quite well understood. Further, recent applications of cavitation involve closely spaced bubbles in strong driving fields in which secondary Bjerknes force dominates over the primary Bjerknes force [14, 15].

The secondary Bjerknes force is attractive when bubbles oscillate in phase, and repulsive for out of phase oscillations. According to the linear Bjerknes theory, attraction occurs when the frequency of the driving acoustic field lies between the the Minnaert (linear-resonance) frequencies of the two bubbles [12]. The Bjerknes force is attractive otherwise. The sign reversal of the secondary Bjerknes force from attraction to repulsion is quite rare. It was experimentally confirmed more than a decade after its theoretical prediction [16]. Zabolotskaya predicted the sign reversal using the linear Bjerknes theory, and attributed it to the change in the oscillation frequency of the bubbles due to bubble-bubble interaction [17]. Similar results were also obtained by Oguz and Prosperetti but using nonlinear theory [18]. However, their theory could not predict the formation of *bubble-grape* like stable structures if bubbles larger than the resonant sizes were closely-spaced in a weak acoustic field. This was contrary to the experimental observations [19].

In contrast, Pelekasis and Tsamopoulos included shape deformations due to subharmonic resonances, and predicted repulsive forces for closely-spaced asymmetric bubble-pairs [20]. But, though their result was in agreement with the linear theory, they attributed the sign reversal to the nonlinear coupling between the bubbles. Doinikov took multiple scattering into account and described the sign reversal due to change in effective resonance frequencies that arises from the stiffening due to in-phase oscillations of the bubbles [21]. The second-order harmonics generated in strong acoustic fields may also yield a sign reversal [22]. Ida

showed that sign reversal could occur in asymmetric bubble-pairs due to the second-highest transition frequency of the smaller bubble [23]. Doinikov further used Lagrangian formalism to obtain sign reversal in bubble-pairs separated by large distances in a strong driving field [24]. In comparison to Doinikov’s approach of including third-order terms, Harkin showed the importance of fourth order terms in the generation of radial harmonics and nonlinear phase shifting, that leads to the sign reversal [25]. Clearly, this indicates the importance of higher order terms in the study of bubble dynamics.

An alternative mechanism for sign reversal based on the linear theory was recently presented in Ref. [26] which seems similar to that from Feuillade [27]. There, the coupled bubble system is shown to have two modes of oscillations: symmetric and asymmetric. Contrary to the symmetric mode that dominates at a resonance close to the resonance frequency of the larger bubble, the antisymmetric mode comes into play at a resonance close to the resonance frequency of the smaller bubble. The symmetric and antisymmetric modes give rise to attractive secondary Bjerknes force and repulsive secondary Bjerknes force respectively.

Thus, it can be inferred that the nonlinearity inherent in bubble dynamics make them a subject difficult for investigation [28, 29]. This can be ascertained from the fact that the study of bubble dynamics has benefited chaos theory, and vice-versa [29–31]. Bubble-systems are known to display chaotic oscillations through period doubling [3, 32]. Similarities between bifurcation diagrams from different bubble-systems have been observed if the ratio of the equilibrium radius to the wavelength of the sound wave is same in them [33]. Interestingly, the presence of charge on a bubble may advance the bifurcations [34]. But, a bubble can only carry a finite charge since there is a minimum radius that it could attain during its collapse phase. Since the charges on a bubble reduces its surface tension, a charged bubble may grow to a relatively larger radius, and also contract to a smaller radius. Charged bubbles also have a greater collapse velocity and a lower Blake threshold [35]. Poincaré maps have further confirmed that bubbles that are slightly smaller than the resonance size oscillates chaotically in both radial and the translational directions [36]. Though, the chaos observed in the translational direction is attributed to the nonlinear radial oscillations. An attractor may exhibit fractality too [32].

The goal of this paper is to investigate strong nonlinear coupling in a two-bubble system which is the simplest case of a bubble cluster. The motivation behind this study is three-fold. First, cavitation bubbles do not occur in isolation, but rather they come in ensembles or clusters. Such clusters are characterized by multi-bubble dynamics which makes their modeling difficult, both analytically and computationally [37]. The possibility of a bubble cluster to originate from a single bubble [9], and multibubbles coalescing to form a single bubble, indicates the importance of nonlinear coupling between bubbles [38]. Besides, the nonlinear interactions in a bubble cloud could lower the subharmonic resonance frequency as well the corresponding minimum pressure threshold that leads to the emission of such subharmonics [39]. On the one hand, nonlinear coupling between bubbles has been ignored by approximating a bubble cluster as a single bubble [40]. On the other hand, this may not be

valid at high frequencies, and in narrow bubble size distributions as then there is a significant increase in the individual scattering cross-section [27]. Besides, the coupling effects between bubbles separated by small distances in stronger acoustic field may be significant enough to alter the behavior of the whole cluster [41]. Unfortunately, the nonlinearity in bubble-dynamics is mostly approximated by the use of linear theories [28, 42]. The inadequacy of such an approach has already been accepted by the scientific community [13, 38, 43, 44]. Alternatively, coupling effects are ignored by assuming bubbles to be separated by a distance much larger than their individual sizes [45]. In such cases, linear superposition of the responses from the individual bubbles is considered identical to the collective response of the bubble cluster, which may not be valid for many applications [43].

The coupling between bubbles is also known to affect the bubble-size distribution within a cluster [46], and therefore statistical techniques have been applied to study such coupling effects [47]. Since, bubble-clusters facilitate a greater number of reaction sites, an understanding of bubble-bubble interactions may give an insight into the factors that lead to the difference in temperature that is observed in sonoluminescence from single bubble and multibubbles [48]. It has also been experimentally shown that the secondary Bjerknes force favors the formation of bubble-clusters instead of dendritic filament branches which alters the sonoluminescence intensity [49]. Thus, the study of multibubble dynamics may benefit sonochemical engineering applications where quenching of sonoluminescence is frequently encountered [29, 50, 51]. Moreover, the coupling between the bubbles play an important role in the generation of shock waves and broadband cavitation noise from the collapse of bubble clouds [52–55]. Such bubble-clouds are regularly generated from ship propellers, and from the firing of air guns in marine seismic explorations [56, 57]. A complete understanding of the nonlinear coupling is essential in the designing of efficient propellers and gun-arrays as they have direct implications for underwater navigation and communication.

Second, some recent experimental studies have shown that bubbles of different sizes when separated by a small distance lead to strong nonlinear coupling [37, 55, 58]. Such a case was examined in Ref. [44] using bi-spherical coordinates, but that was restricted to small amplitude oscillations. A relatively successful theory of nonlinear coupling between bubbles was presented in Ref. [59] almost twenty years ago which also motivates the study presented in this paper. However, Keller-Miksis equations (KMEs) derived to describe the bubble-bubble interaction in Ref. [59] were based on assumptions that could be valid only for weak coupling. That would be plausible either under the action of a weak acoustic field, or, when bubbles are far apart from each other. An evidence of weak coupling can be seen from Fig. 5(b) in Ref. [59] where the radius evolution of the larger bubble remains unaffected from the smaller bubble at all times. Such an assumption of weak coupling was reasonable for applications twenty years ago. But modern applications involve bubbles in immediate vicinity of each other. Some examples can be seen in Fig. 12 in Ref. [7] for shock wave lithotripsy, Fig. 2 in Ref. [8] for sonoporation, Fig. 2 in Ref. [9] for microfluidics, and Fig. 4 in Ref. [11] for cleaning. Moreover, most equations proposed to study single and multibubble

dynamics are modifications of the Rayleigh-Plesset equation that takes into account the convective contribution from the Navier-Stokes equation (NSE) in its derivation [6, 43, 60]. But, the theories that are currently used to study radiation-coupling effects between bubbles seem to have ignored this because of the analytic and computational complexities that comes along with the higher order terms. Thus, contrary to the relevance of the higher order terms in cavitation-like highly nonlinear dynamic process [25, 61], they were ignored in Ref. [59]. Thus, in light of this observation, the theory from Ref. [59] will be regarded as the theory of weak nonlinear coupling in the rest of this paper.

Third, there is no clear consensus on what leads to the asymmetry in the secondary Bjerknes force. A time-delay in radiation due to the large separation between the bubbles has been predicted as one of the possible causes for it in Ref. [59]. Another possibility as mentioned in Ref. [62] is asymmetric viscous dissipation of the forces for bubbles of different sizes. But, since the fluid was assumed to be inviscid in that study, the authors had themselves admitted it to be counter-intuitive.

The rest of the article is organized as follows. Sec. II is divided into two subsections. In its first subsection, the established theory of weak nonlinear coupling [59], is briefly summarized. In the second subsection, the theory of strong nonlinear coupling is developed and subsequently a system of strongly coupled KMEs is derived. The numerical solutions of the KMEs are presented in Sec. III where they are also compared with the solutions from the weak nonlinear coupling. Finally, in Sec. IV, the implications of this work is discussed.

## II. NONLINEAR COUPLING BETWEEN A PAIR OF BUBBLES

It is assumed that two cavitation-bubbles with volumes  $V_1$  and  $V_2$ , are formed in an incompressible fluid of density,  $\rho$ , and dynamic viscosity,  $\mu$ . The two bubbles referred as  $B1$  and  $B2$ , have the radii  $R_1(t)$  and  $R_2(t)$  respectively, and are separated by a distance,  $d$ , that is measured from the bubble centers. The radial velocities of the bubble boundaries at any given time,  $t$ , are then expressed as,  $\dot{R}_1(t)$  and  $\dot{R}_2(t)$ , where the number of over-dots represent the order of differentiation with respect to time. So, a double-dot, and a triple-dot over  $R$  would imply an acceleration and  *jerk* of the bubble boundaries respectively. Similar to Refs. [44, 59], the bubbles are assumed spherical in shape which is valid for bubbles smaller than the wavelength of the acoustic wave that excites it. So, scattering effects are neglected too. Also, thermal and viscous dissipation are ignored.

The fluid flow during cavitation can safely be assumed radially symmetric. Therefore, the continuity equation in the spherical coordinate system contains contribution only from the radial-components of the flow, none from azimuthal and polar parts. Consequently,

$$u_1 = \left( \frac{R_1}{r} \right)^2 \dot{R}_1, \quad (1)$$

where  $r$  is the distance from the center of the  $B1$ , and  $u_1$  is the radial velocity of the fluid

in the immediate vicinity of the boundary of  $B1$ . Further, the nonlinear coupling theory developed in this paper builds on the modified KME [59], which is expressed for  $B2$  as:

$$\left(1 - \frac{\dot{R}_2}{c}\right) R_2 \ddot{R}_2 + \frac{3}{2} \dot{R}_2^2 \left(1 - \frac{\dot{R}_2}{3c}\right) = \left(1 + \frac{\dot{R}_2}{c}\right) \frac{P}{\rho} + \frac{R_2}{\rho c} \frac{dP}{dt}, \quad (2)$$

where  $P = P_{\text{bw}} - P_{\text{stat}} + P_v - P_{\text{ext}}$ . Here,

$$P_{\text{bw}} = \left(P_{\text{stat}} - P_v + \frac{2\sigma}{R_{20}}\right) \left(\frac{R_{20}}{R_2}\right)^{3\gamma} - \frac{2\sigma}{R_2} - 4\mu \frac{\dot{R}_2}{R_2}, \quad (3)$$

where  $R_{20}$  and  $\sigma$  are the equilibrium radius and surface tension of  $B2$  respectively,  $c$  is the sound speed in water,  $\gamma$  is the polytropic index of the gas inside  $B2$ ,  $P_{\text{bw}}$  is the liquid pressure at the bubble wall,  $P_{\text{stat}}$  is the hydrostatic pressure far away from  $B2$ ,  $P_v$  is the vapor pressure, and  $P_{\text{ext}} = P_s \sin[2\pi f_s (t + (R_2/c))]$  is the time-delayed external driving acoustic field of amplitude,  $P_s$ , and frequency,  $f_s$ .

### A. Weak nonlinear coupling

The framework presented to study weak nonlinear coupling in bubbles in Ref. [59], is summarized here. If  $p_1$  is the pressure set-up by an oscillating bubble,  $B1$ , around its surrounding fluid, then from Eq. (3) in Ref. [59], we have

$$p_1 = \frac{\rho}{r} \left(2R_1 \dot{R}_1^2 + R_1^2 \ddot{R}_1\right). \quad (4)$$

The radiation force exerted by  $B1$  on  $B2$  is then (see Eq. (5) in Ref. [59])

$$F_{12}^w = \frac{\rho V_2}{4\pi d^2} \frac{d^2 V_1}{dt^2} \hat{e}_r, \quad (5)$$

where,  $\hat{e}_r$  denotes the radial unit vector, and the superscript “ $w$ ” symbolizes the weak nonlinear coupling aspect of the force. The secondary Bjerknes force,  $F_B^w$ , is calculated by time-averaging the radiation force as (see Eq. (6) in Ref. [59])

$$F_B^w = \langle F_{12}^w \rangle = -\frac{\rho}{4\pi d^2} \langle \dot{V}_1 \dot{V}_2 \rangle \hat{e}_r, \quad (6)$$

where  $\langle \cdot \rangle$  denotes time-averaging over a period of the incident wave. The attractive and repulsive nature of the time-averaged secondary Bjerknes force are respectively represented by their negative and positive signs. It can be seen from Eq. (6) that interchanging the indices  $1 \leftrightarrow 2$  does not change the expression on the right hand side. Thus, the secondary Bjerknes force is symmetric in the same coordinate system as

$$\langle F_{12}^w \rangle = -\langle F_{21}^w \rangle. \quad (7)$$

Replacing  $P_{\text{ext}}$  in Eq. (2) by  $P_{\text{ext}} + p_1$ , and then substituting Eq. (4) in it, the governing KME for  $B2$  is obtained as (see Eq. (07) in Ref. [59])

$$\left(1 - \frac{\dot{R}_2}{c}\right) R_2 \ddot{R}_2 + \frac{3}{2} \dot{R}_2^2 \left(1 - \frac{\dot{R}_2}{3c}\right) = \left(1 + \frac{\dot{R}_2}{c}\right) \frac{P_{\text{bw}} - P_{\text{stat}} + P_v - P_{\text{ext}}}{\rho} + \frac{R_2}{\rho c} \frac{d}{dt} [P_{\text{bw}} - P_{\text{ext}}] - C_2^w, \quad (8)$$

where the *coupling dose*,  $C_2^w$ , received by  $B2$  from  $B1$  is

$$C_2^w = \frac{1}{d} \left(2R_1 \dot{R}_1^2 + R_1^2 \ddot{R}_1\right). \quad (9)$$

The motivation to call the last term in Eq. (9) as coupling dose is due to its units,  $J/kg$ .

## B. Strong nonlinear coupling

The Navier-Stokes equation (NSE) for a purely radial flow due to the pulsations of  $B1$  is

$$\frac{Du_1}{Dt} \equiv \frac{\partial u_1}{\partial t} + u_1 \frac{\partial u_1}{\partial r} = -\frac{1}{\rho} \frac{\partial p_1}{\partial r} + \frac{\mu}{\rho} \left[ \frac{1}{r^2} \frac{\partial}{\partial r} \left( r^2 \frac{\partial u_1}{\partial r} \right) - \frac{2u_1}{r^2} \right] + f_{\text{ext}}, \quad (10)$$

where  $D/Dt$  is the material derivative operator expressed as the sum of an instantaneous local (time) derivative and a convective (spatial) derivative, and  $f_{\text{ext}}$  represents external body forces such as gravity, Lorentz force, etc, that could be affecting the flow. The spatial-derivative term describes the acceleration that one observes while moving radially along the velocity flow field,  $u_1$ . And, the time-derivative term describes the intrinsic variation of the field. It should be noted that contrary to the local acceleration which is zero for steady flow, i.e., when  $u_1$  is constant in time, the convective acceleration may be non-zero. Though, the convective contribution diminishes rapidly for most fluid flows in their far field, it may play a major role in the near field. Since,  $u_1 \cdot \partial u_1 / \partial r = \partial u_1^2 / 2 \partial r$ , the convective term is the main source of nonlinearity that may also lead to chaos and turbulence. Therefore, it is only natural to include the convective contribution in order to explore the complete nonlinearity.

Further, since shear viscosity does not generate any resistance in a purely radially symmetric flow around a bubble, viscous term vanishes off completely from the NSE. But, as shown in Eq. (3), there is some viscous contribution that comes from the shear stress at the bubble boundary. The local and convective derivative terms of Eq. (10) are obtained by applying appropriate derivative operators on Eq. (1). Substituting the derivative terms back in Eq. (10), and assuming,  $f_{\text{ext}} = 0$ , we get

$$\frac{1}{r^2} \left(2R_1 \dot{R}_1^2 + R_1^2 \ddot{R}_1\right) - \frac{2R_1^4 \dot{R}_1^2}{r^5} = -\frac{1}{\rho} \frac{\partial p_1}{\partial r}. \quad (11)$$

Integrating Eq. (11) on both sides with respect to  $r$ , gives

$$p_1 = \rho \left[ \frac{1}{r} \left(2R_1 \dot{R}_1^2 + R_1^2 \ddot{R}_1\right) - \frac{R_1^4 \dot{R}_1^2}{2r^4} \right]. \quad (12)$$

Interestingly, the importance of the two terms in Eq. (12) has been acknowledged in Ref. [60], where the first term that is inversely proportional to  $r$  was found important near bubble minima such that it accounts for the primary shock wave pressure and subsequent pressure peaks. The second term that is inversely proportional to the fourth power in  $r$  was termed as the “*afterflow*” pressure which is important between pressure peaks at small distances from the bubble. It should be clarified that the afterflow term stems from the convective acceleration of the fluid. Unfortunately, this term was ignored in Eq. (4) to develop the theory of weak nonlinear coupling in Ref. [59]. Though such an approach is quite acceptable for small amplitude oscillations [63], convective contribution may become significant for large amplitude nonlinear oscillations where they may also give rise to microstreaming like second order effects [64]. The pressure gradient,  $\partial p_1/\partial r$ , set-up radially outward by  $B1$  is experienced as a radiation force,  $F_{12}^s$ , which is expressed as

$$F_{12}^s = -V_2 \frac{\partial p_1}{\partial r} \Big|_{r=d} \hat{e}_r, \quad (13)$$

where the superscript “*s*” symbolizes the strong nonlinear coupling aspect of the force. Extracting  $\partial p_1/\partial r$  from Eq. (11) and substituting it in Eq. (13), we get

$$F_{12}^s = \rho V_2 \left[ \frac{1}{d^2} \left( 2R_1 \dot{R}_1^2 + R_1^2 \ddot{R}_1 \right) - \frac{2R_1^4 \dot{R}_1^2}{d^5} \right] \hat{e}_r, \quad (14)$$

which can also be expressed in terms of bubble volumes as

$$F_{12}^s = \frac{\rho V_2}{4\pi d^2} \left[ \frac{d^2 V_1}{dt^2} - \frac{1}{2\pi d^3} \left( \frac{dV_1}{dt} \right)^2 \right] \hat{e}_r. \quad (15)$$

The secondary Bjerknes force,  $F_B^w$ , is estimated by time-averaging  $F_{12}^s$  from Eq. (15) over the time-period,  $\tau$ , of the driving acoustic field as

$$F_B^s = \langle F_{12}^s \rangle = \frac{\rho}{4\pi d^2} [I_1 - I_2] \hat{e}_r, \quad (16)$$

where

$$I_1 = \frac{1}{\tau} \int_t^{t+\tau} V_2(t') \frac{d^2 V_1(t')}{dt'^2} dt', \quad I_2 = \frac{1}{2\pi d^3} \frac{1}{\tau} \int_t^{t+\tau} V_2(t') \left( \frac{dV_1(t')}{dt'} \right)^2 dt, \quad (17)$$

and  $t'$  is the dummy variable of integration. Evaluating the integrals in Eq. (17), and substituting them back in Eq. (16), we get

$$F_B^s = \langle F_{12}^s \rangle = -\frac{\rho}{4\pi d^2} \left[ \langle \dot{V}_1 \dot{V}_2 \rangle + \frac{1}{2\pi d^3} \langle \dot{V}_1^2 V_2 \rangle \right] \hat{e}_r. \quad (18)$$

There are three main differences that can be observed on comparing Eqs. (15) and (18) that are obtained for the secondary Bjerknes force from strong nonlinear coupling, with the

respective Eqs. (5) and (6) obtained from the weak nonlinear coupling. First, the presence of the last term in Eq. (18) revokes the symmetry restrictions of the Bjerknes force as

$$\langle F_{12}^s \rangle \neq -\langle F_{21}^s \rangle. \quad (19)$$

It will be further shown in the next section that the asymmetry is observed in the magnitude as well as in the sign reversal of the Bjerknes force. An interesting finding is that  $\langle F_{12}^s \rangle$  and  $\langle F_{21}^s \rangle$  may not necessarily be equal even in a symmetric bubble-pair, i.e., when  $V_1 = V_2$ . This is because identical bubbles may not have the same radial velocity if the coupling between them is nonlinear. But, the symmetry of the Bjerknes force could be restored if the bubbles are separated by a sufficiently large distance,  $d$ , such that the convective contribution from the last term in Eq. (18) becomes negligible.

Second, contrary to most studies in which secondary Bjerknes force is assumed to have an inverse square law form along the lines of gravitational, electrostatic, and magnetic force [12], it is observed that such an assumption may not be valid if there is a major contribution from the convective term in Eq. (18). This may happen in the case of closely-spaced bubbles as then the bubbles are strongly coupled and influence each-other's oscillations significantly [23, 26]. Interestingly, this limitation of the Bjerknes force was also *subtly* mentioned by Crum in the paragraph following Eq. (6) in Ref. [12].

Third, the generalized observation made about the local and spatial derivative terms in the paragraph following Eq. (10) can also be verified from the expressions of the Bjerknes force. In the case when  $B1$  has a constant velocity, i.e.,  $\dot{u}_1(t) = 0$ , then following the classical notion from Newton's second law, no force would be exerted from  $B1$  to any other bubble in its neighborhood. This corresponds to the case of  $\ddot{V}_1 = 0$ , which yields  $F_{12}^w = 0$  from Eq. (5). Further,  $F_{21}^w = 0$ , due to the symmetry restriction from Eq. (7). But, contrary to this expectation from the classical mechanics, even in the case when  $\ddot{V}_1 = 0$ , the presence of the last term from the convective contribution in Eq. (15) guarantees an attractive force,  $F_{12}^s < 0$ , on  $B2$  due to  $B1$ . Thus, as mentioned in Ref. [43], it may be difficult to *directly* relate the convective contribution to the radiation field in a classical sense. Further, since  $\dot{V}_1$  is squared in the last term in Eq. (15), its contribution to the Bjerknes force always remains attractive at all instants of the driving sound field. Consequently, the convective (*afterflow*) contribution adds to the attraction between the bubbles, but opposes their mutual repulsion.

The response of a bubble to the acoustic field emanated by another bubble is similar in principle in the way it reacts to the external driving pressure,  $P_{\text{ext}}$ . So, for  $B2$ , we have,  $P = P_{\text{bw}} - P_{\text{stat}} + P_v - (P_{\text{ext}} + p_1)$ , where  $p_1$  given by Eq. (12) is evaluated at  $r = d$ . Substituting this expression for  $P$  in Eq. (2), we arrive at the final governing KME for  $B2$  that encompasses the strong nonlinear coupling effects from  $B1$  as

$$\left(1 - \frac{\dot{R}_2}{c}\right) R_2 \ddot{R}_2 + \frac{3}{2} \dot{R}_2^2 \left(1 - \frac{\dot{R}_2}{3c}\right) = \left(1 + \frac{\dot{R}_2}{c}\right) \frac{P_{\text{bw}} - P_{\text{stat}} + P_v - P_{\text{ext}}}{\rho} + \frac{R_2}{\rho c} \frac{d}{dt} [P_{\text{bw}} - P_{\text{ext}}] - C_2^s, \quad (20)$$

where the strong coupling dose,  $C_2^s$ , can be grouped as the sum of three terms;  $C_2^s = T_1 + T_2 + T_3$ . The three terms are:

$$T_1 = \frac{1}{d} \left( 2R_1 \dot{R}_1^2 + R_1^2 \ddot{R}_1 \right), \quad (21)$$

$$T_2 = \frac{1}{cd} \left( 2\dot{R}_2 R_1 \dot{R}_1^2 + \dot{R}_2 R_1^2 \ddot{R}_1 + 2R_2 \dot{R}_1^3 + 6R_2 R_1 \dot{R}_1 \ddot{R}_1 + R_2 R_1^2 \ddot{\ddot{R}}_1 \right), \quad (22)$$

$$\text{and } T_3 = -\frac{1}{2cd^4} \left( cR_1^4 \dot{R}_1^2 + \dot{R}_2 R_1^4 \dot{R}_1^2 + 4R_2 R_1^3 \dot{R}_1^3 + 2R_2 R_1^4 \dot{R}_1 \ddot{R}_1 \right). \quad (23)$$

It can be seen that the term  $T_1$  has the same expression as the coupling dose term,  $C_2^w$ , in Eq. (9) from weak nonlinear coupling. The respective KME for  $B1$  can be obtained by interchanging the indices  $1 \leftrightarrow 2$  in the set of Eqs. (20)-(23). The presence of the jerk term,  $\ddot{\ddot{R}}_1$ , in Eq. (22) is not new in the study of bubble dynamics. On the one hand, it has been shown that a jerk equation is equivalent to a system of three first order, ordinary, non-linear differential equations which is a minimal setting for chaotic solutions [65]. Thus, the observation of chaotic oscillations is not surprising in multi-bubble systems [29, 31]. On the other hand, the jerk-term also invokes Ostrogradsky's instability [66].

### III. NUMERICAL RESULTS AND DISCUSSION

It is assumed that the gas bubbles undergo adiabatic oscillations in water. So, the numerical values used for the physical variables are:  $P_{\text{stat}} = 1 \text{ bar} = 101.325 \text{ kPa}$ ,  $P_v = 2.3388 \text{ kPa}$ ,  $\sigma = 0.0728 \text{ N/m}$ ,  $\rho = 998.207 \text{ kg/m}^3$ ,  $\mu = 0.001002 \text{ kg/(ms)}$ ,  $c = 1481 \text{ m/s}$ , and  $\gamma = 1.4$ . The jerk-term in Eq. (22) is neglected to circumvent the Ostrogradsky instability in numerical solutions. An approximation of the jerk-term could be possible [10, 43, 44], but it is avoided because of the skewedness from the approximation error that leads to the non-convergence of the numerical algorithms used to solve the KMEs [67].

The set of coupled KMEs is solved for both weak nonlinear coupling and strong nonlinear coupling for three bubble-pairs that are under excitation from acoustic fields of different strengths and frequencies. The bubble-pairs are: (6, 5), (10, 5), and (112, 22), where the two numeric values inside the parentheses are the equilibrium radius of  $B1$ , and  $B2$ , in  $\mu\text{m}$ , respectively. Such a choice for bubble-pairs is driven by two reasons. First, the pairs (6, 5) and (10, 5) are also studied in Ref. [59]. Therefore, a direct comparison of the results from weak nonlinear and strong coupling is possible. And, the experimental observation of the third pair (112, 22) against the predictions from the linear Bjerknes theory [13], will further provide a validation of the results from strong nonlinear coupling. Besides Ref. [13], there is experimental observation of repulsive secondary Bjerknes force in Ref. [26] too, but the data from the latter cannot be used for validation. It is because the pressure reported in Ref. [26] is in volts which cannot be directly converted into pascals due to the complexity of the experimental procedure. The second reason is the relatively low

linear resonance frequencies,  $f_m$ 's, for the three pairs that are approximately, [463, 555], [277, 555], and [25, 126] respectively, where the numeric values inside the square brackets are in kHz. Such values of the resonance frequencies help ensure negligible time-delay between the bubbles which would otherwise further complicate the bubble-bubble interaction. The maximum time-delay for the first two pairs are, 0.2 % and 0.3 % of the time-period of the highest frequency of operation of 30 kHz. For the third pair, the maximum delay is close to 1.3 % of the time-period of the wave operation at 27 kHz. Also, the different sizing of the bubbles allow an investigation of the nonlinear coupling in bubble-pairs with different degree of asymmetry as the ratio of equilibrium radii,  $R_{10}/R_{20}$ , for the three pairs are approximately, 1.2, 2, and 5 respectively. Moreover, the bubble-sizes investigated here have a higher probability of occurrence within the assumed physical conditions, see Fig. 1 in [59].

As shown in Table I, the distance between the first two pairs is kept four times their combined equilibrium radii at pressure magnitudes of 0.7 atm and 1 atm. The distance is increased to ten times their combined equilibrium radii at 1.3 atm. This ensures that the separation between the bubbles is always greater than the combined radii of the two bubbles at any instant. The same approach is adopted in Ref. [59] as well to avoid losing the sphericity of bubbles. But, in strong driving fields ( $> 1$  atm), sphericity is most probably lost. The resulting shape oscillations may also exchange energy with the volume oscillations, but for micrometer size bubbles the implications from such coupling are quite small [29, 68]. Besides, the bubble cavitation becomes transient if the separation distance is reduced to less than eight times their combined radii under very strong driving fields,  $P_s \geq 1.3$  atm. This is expected as bubbles may then grow into each other during their maximum growth phase which will immediately affect their stability and sphericity. This will also risk the generation of micro-jets if bubbles touched each other at opposite phases [15, 68]. In such a transient cavitation collapse, a bubble often disintegrates into a collection of smaller bubbles. Further, depending on the driving conditions and the magnitude of the secondary Bjerknes force, the bubbles may coalesce together if the force is attractive [14, 18]. It is evident that for problems involving bubbles separated by very small distances in very strong fields, the framework of KMEs may not be reliable. Rather, boundary element methods should be preferred [68]. Moreover, since the focus of this paper is to study Bjerknes force in stable cavitation, effects like jetting, formation of capillary waves and shock waves that mostly occur during the violent phases of transient cavitation, are not pursued here. All bubble-pairs in this study exhibited stable cavitation, at least for five to ten wave cycles.

A distinction between near field and far field that is also found relevant in this study is provided by Prosperetti in Ref. [69]. The near field extends to a distance that is of the same order as the bubble radius. And, the far field scales as,  $c \cdot \tau$ . The far field results from strong nonlinear coupling and weak nonlinear coupling are almost identical. Therefore, they are neither shown, nor discussed here. Also, chaotic behavior was not observed in this study.

The numerical results for the secondary Bjerknes force are summarized in Table I. For the first two bubble pairs, (6, 5), and (10, 5), the weak nonlinear coupling always results into a

net attractive force between the bubble. This is in agreement with the linear Bjerknes theory as both bubbles are weakly driven below their resonance frequencies. But, strong coupling predicts both attractive and repulsive force. Also, strong nonlinear coupling gives a greater magnitude of the secondary Bjerknes force than that from the weak nonlinear coupling. The weaker the strength of the driving field, the larger the difference in magnitude of the forces is observed, often by more than two orders of magnitude. Further, the symmetry restrictions on weak coupling yield almost same magnitude and sign of the mutual Bjerknes force, though minor differences can be observed in strong driving field of 1.3 atm. On the contrary, the strong coupling leads to both asymmetry in magnitude as well as asymmetry in sign reversal of the Bjerknes force. In the case of symmetric sign reversal, i.e., when both  $\langle F_{12} \rangle$  and  $\langle F_{21} \rangle$  are positive, both bubbles repel each other. In contrast, in the case of asymmetric sign reversal, one of the bubbles exerts an attractive force on the second bubble, but the second bubble exerts a repulsive force on the first bubble. An example of this is the first pair (6, 5) separated by a distance of 44  $\mu m$  under excitation by a sound field of strength of 0.7 atm, and frequency, 20 kHz. The resulting values of  $\langle F_{12}^s \rangle$  and  $\langle F_{21}^s \rangle$  are +1.4  $\mu N$  and -0.03  $\mu N$  respectively. Such a situation would correspond to a *bubble-bubble chase* like phenomena where the first bubble is attracted by the second bubble, but the latter is repelled by the former. In such a situation, the final behavior of the bubble-pair would be determined by the resultant,  $\langle F_{12}^s \rangle + \langle F_{21}^s \rangle$  as shown in the last column of the Table I, which in this case will be a repulsion. Such a case of bubble-pair translation has recently been predicted using the boundary element method [68], but primary Bjerknes force was attributed for it. This is because the secondary Bjerknes force has traditionally been considered to yield either attraction, or, repulsion. Besides the asymmetry in the sign reversal, large inequality in the magnitude of the mutual Bjerknes force is also observed in strong coupling. It should be emphasized that contrary to the possibility of asymmetry in the Bjerknes force due to time delay [59] and viscous dissipation [62], here it arises from the strong nonlinear coupling between bubbles. Thus, a complete understanding of the strong coupling is required. Otherwise, the effects from the secondary Bjerknes force could be mistaken as that from the primary Bjerknes force, and vice-versa.

The bubbles in the third pair (112, 22), with a separation of 450  $\mu m$ , has been experimentally observed to attract each other when excited by a sound field of strength, 0.03 atm, and frequency, 27 kHz [13]. Since the exciting frequency is in between the linear resonance frequencies of the two bubbles, the bubbles were expected to repel each other in accordance to the linear Bjerknes theory. But instead the bubbles attracted each other. Both weak coupling theory and strong coupling theory predict attractive Bjerknes force as documented in Table I. But, the observed repulsive force was much greater than the predictions from the linear theory, though the exact value is not mentioned. Since strong coupling yields a relatively larger magnitude of the Bjerknes force than that from the weak coupling, the findings may be seen as inclined in its favor. Further, it is reasonable to expect that bubbles of such large size-difference may not exert the same magnitude of force on each other that

$(R_{10}, R_{20})$ ( $\mu m$ )	$d$ ( $\mu m$ )	$P_s$ (atm)	$f_s$ (kHz)	$\langle F_{12} \rangle$ ( $\mu N$ )	$\langle F_{21} \rangle$ ( $\mu N$ )	$\langle F_{12} \rangle + \langle F_{21} \rangle$ ( $\mu N$ )
(6, 5)	44	0.7	20	+1.4 (−0.00008)	−0.03 (−0.00008)	+1.37 (−0.00016)
			25	+1.3 (−0.00013)	−0.2 (−0.00013)	+1.1 (−0.00026)
			30	+1.25 (−0.00019)	−0.25 (−0.00019)	+1 (−0.00038)
		1	20	+1.36 (−0.007)	+0.01 (−0.007)	+1.37 (−0.014)
			25	+1.1 (−0.01)	−0.5 (−0.01)	+0.6 (−0.02)
			30	+1.1 (−0.01)	−0.7 (−0.01)	+0.4 (−0.02)
	110	1.3	20	−2.2 (−6.4)	−6.4 (−5.5)	−8.6 (−11.9)
			25	+5.7 (−3.2)	−2.3 (−3.7)	+3.4 (−6.9)
			30	−4 (−1.9)	−7.2 (−1)	−11.2 (−2.9)
(10, 5)	60	0.7	20	+0.03 (−0.00024)	+0.14 (−0.00024)	+0.17 (−0.00048)
			25	−0.06 (−0.0004)	−0.26 (−0.0004)	−0.32 (−0.0008)
			30	−0.1 (−0.00052)	−0.4 (−0.00061)	−0.5 (−0.00113)
		1	20	−0.4 (−0.03)	+0.05 (−0.03)	−0.35 (−0.06)
			25	+0.6 (−0.03)	−1 (−0.03)	−0.4 (−0.06)
			30	+0.9 (−0.03)	−1.7 (−0.03)	−0.8 (−0.06)
	150	1.3	20	−3.3 (−4)	−10.2 (−6.6)	−13.5 (−10.6)
			25	+7 (−2.1)	−4.3 (−3.4)	+2.7 (−5.5)
			30	−3.9 (−1.1)	−8.4 (−2.1)	−12.3 (−3.2)
(112, 22)	450	0.03	20	−2.3 (−0.003)	−21.7 (−0.003)	−24 (−0.006)
			25	−2.9 (−0.02)	−26.2 (−0.01)	−29.1 (−0.03)
			27	−3 (−0.02)	−27 (−0.01)	−30 (−0.03)
		0.1	20	−2.1 (−0.02)	−21.5 (−0.02)	−23.6 (−0.04)
			25	−2.8 (−0.1)	−26.3 (−0.06)	−29.1 (−0.16)
			27	−3 (−0.07)	−27 (−0.06)	−30 (−0.13)
	700	0.4	20	−0.7 (−0.1)	−9.2 (−0.1)	−9.9 (−0.2)
			25	−1.3 (−0.17)	−9.2 (−0.17)	−10.5 (−0.34)
			27	−1.4 (−0.1)	−8.1 (−0.15)	−9.5 (−0.25)

TABLE I. Comparison of secondary Bjerknes force obtained from strong nonlinear coupling and weak nonlinear coupling. The values inside the parentheses in the last three columns correspond to the weak nonlinear coupling.

is restricted by the symmetricity conditions of the weak nonlinear coupling. The outcome from the strong nonlinear coupling could have been validated with more authority, if the bigger bubble was not fixed in the experiment as then the strong attractive force exerted by the smaller bubble on the bigger bubble would have been observed.

The radial pulsations of the second bubble pair, (10, 5), is shown in Fig. 1. The critical Blake radii [70] for the bubbles are approximately  $48 \mu m$  and  $18 \mu m$  respectively. It can be seen from Fig. 1(b) that the two bubbles under weak nonlinear coupling at 1 atm, did not grew larger than their respective critical Blake radius, implying stable cavitation. But, as shown in the Fig. 1(a), the smaller bubble,  $B2$ , surpassed its critical Blake threshold at the same driving pressure due to the strong coupling affects from  $B1$ . In contrast, as shown in Figs. 1(c) and (d), both bubbles grew past their respective critical radii because the driving field is sufficiently strong at 1.3 atm. Bubbles that experience growth larger than their critical Blake threshold are known to exhibit nonlinear resonance [59], that is observed in Figs. 1(a), (c), and (d). The physical mechanism underlying such an explosive growth is the interplay between the liquid negative pressure and controlling effects of the surface tension. Further, since surface tension dictates the growth of small cavitation bubbles even more in a weak field, nonlinear resonance growth may not be observed in such cases.

The dramatic growth of the smaller bubble,  $B2$ , beyond its critical Blake radius can be explained using the concept of dynamical Blake threshold [32, 59]. As seen in Fig. 1(a), as the larger bubble,  $B1$ , undergoes its first major collapse just before the end of the first wave cycle, it pulls the fluid surrounding its boundary inward. This convective contribution from the  $B1$  that is best taken care in the framework of strong coupling lowers the liquid pressure surrounding the smaller bubble,  $B2$ . This facilitates an explosive growth of  $B2$  which due to its smaller size easily gets excited even more. This effect is more pronounced either when the bubbles are closely-spaced, or when they are placed in a stronger driving field as shown in Fig. 1(c). It can be seen that the main nonlinear resonance jump of  $B2$  occurs approximately at the same time when  $B1$  undergoes contraction. This aspect which can also be observed in Fig. 1(c) is almost absent in Figs. 1(b) and (d) that are from the weak coupling. Surprisingly, this is in agreement with the findings from Ref. [71] which describes a reduction of the effective cavitation threshold pressure for a smaller bubble in the presence of a larger bubble. Further as seen in Fig. 1(a), a few successive oscillations of  $B1$  after its first major collapse has relatively lesser magnitude when compared to its respective oscillations from Fig. 1(b). This is because of the explosive growth of  $B2$  that pushes the fluid outward, which in turn, increases the liquid pressure surrounding  $B1$ , and hence restrains its growth. In the case of weak coupling, there is no convective acceleration of the fluid which in turn does not alter the critical pressure thresholds.

It should be noted that bubble dynamics after such nonlinear resonance jumps switches drastically from quasi-static oscillations to rapid phases of growth and violent collapses. This is because after the bubble reaches its maximum growth, the internal pressure in the bubble drops so low that it is unable to retain the inward flow of the surrounding liquid. Thereafter, the bubble may also enter a transient phase in which it collapses violently and undergoes rapid successions of afterbounces. In the bubble-pairs tested here, the collapse velocity,  $\dot{R}$ , has been less than  $1 m/s$ ,  $10 m/s$ , and  $100 m/s$  at 0.7 atm, 1 atm, and 1.3 atm respectively. Also, the bubbles have a relatively greater collapse velocity in the case of strong

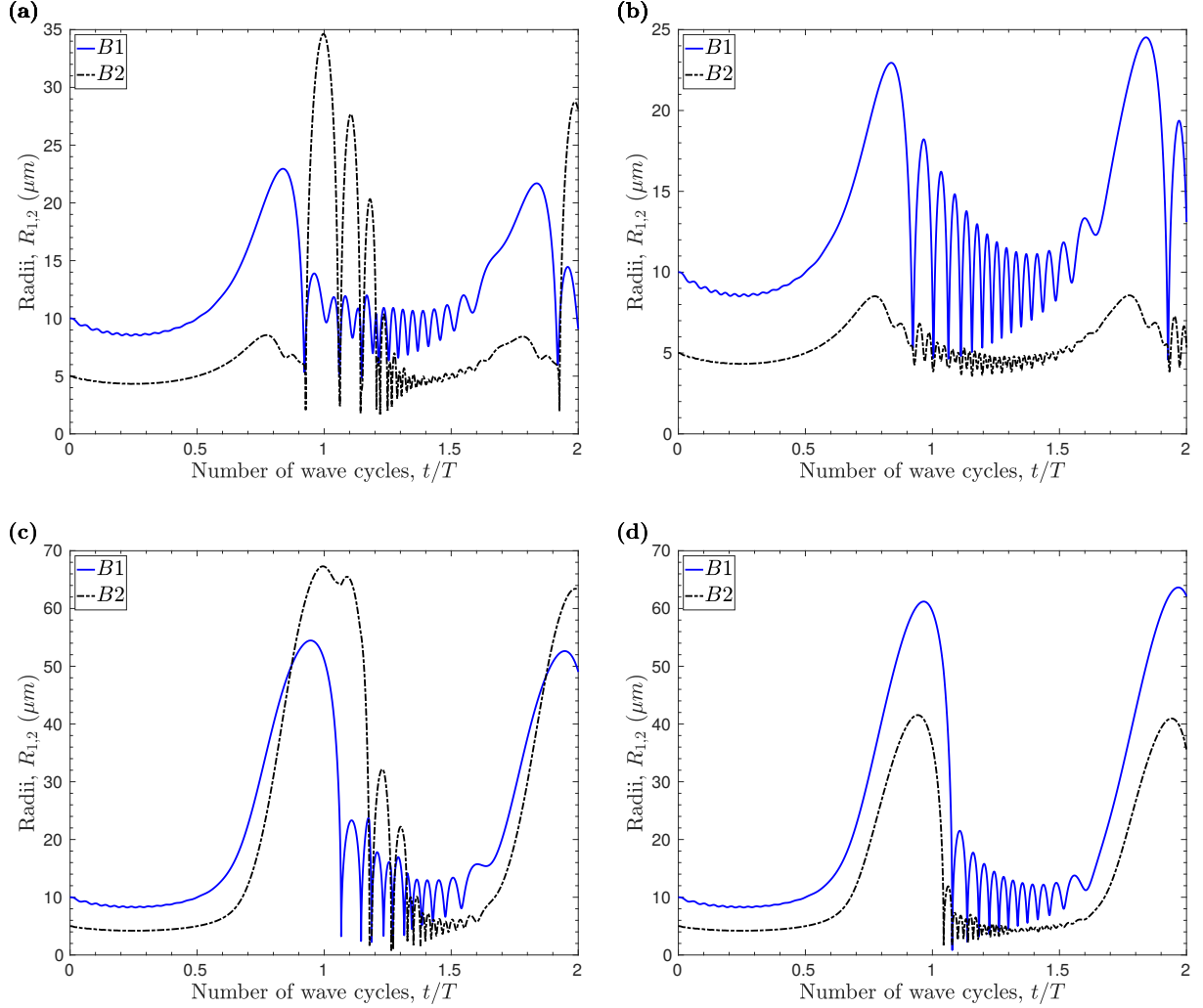


FIG. 1. (Color online) Radii evolution for the bubble-pair;  $B_1$  (solid line) and  $B_2$  (dash-dotted line), with  $R_{10} = 10 \mu m$  and  $R_{20} = 5 \mu m$ , for the first two wave cycles of frequency,  $f_s = 30 \text{ kHz}$ . Subfigures (a) and (c) correspond to strong nonlinear coupling. And, subfigures (b) and (d) correspond to weak nonlinear coupling. The top and bottom rows represent radii evolution at  $P_s = 1 \text{ atm}$ ,  $d = 75 \mu m$ , and  $P_s = 1.3 \text{ atm}$ ,  $d = 150 \mu m$ , respectively.

coupling. Therefore, compressibility effects should be taken into account for closely-spaced bubble-pairs in stronger driving fields. Furthermore, since the ratio,  $f_s/f_m$ , is not an integer for all bubble-pairs, it may lead to ultra-harmonic resonances that could be more pronounced in the strong nonlinear coupling [32].

Another important observation from Fig. 1 is that effects from strong coupling and weak coupling are almost unnoticeable until ninety percent of the first wave cycle, though these effects show-up little earlier at 1.3 atm. This can also be confirmed from Figs. 2(a) and (b), where the ratio of the absolute values of strong coupling dose and weak coupling dose are plotted for the two bubbles. Surprisingly, since the ratio between the doses for the

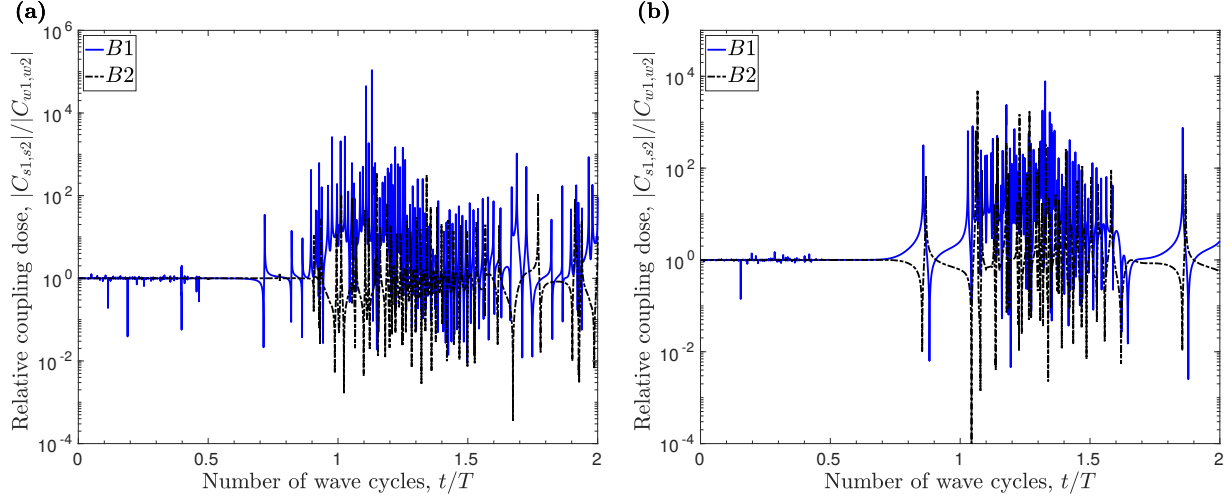


FIG. 2. (Color online) Ratio of coupling dose from strong nonlinear coupling and weak nonlinear coupling for the bubble-pair;  $B_1$  (solid line), and  $B_2$  (dash-dotted line), with  $R_{10} = 10 \mu m$  and  $R_{20} = 5 \mu m$ , for the first two wave cycles of frequency,  $f_s = 30$  kHz. Subfigures (a) and (b) correspond to the conditions,  $P_s = 1$  atm,  $d = 75 \mu m$ , and  $P_s = 1.3$  atm,  $d = 150 \mu m$ , respectively.

smaller bubble,  $B_2$ , is less than one at multiple instances after the first wave cycle, this means that the weak nonlinear coupling is not necessarily lesser in magnitude. But, rather it over-predicts the coupling dose for  $B_2$ . The opposite happens for the bigger bubble,  $B_1$ , for which the weak nonlinear theory under-predicts the coupling dose.

The effects of strong nonlinearity in coupling is best witnessed in the case of symmetric bubble-pair, (8, 8), as shown in Fig. 3. The radii-evolution of the bubbles separated by a distance eight times their combined equilibrium radii, do not look identical even if their equilibrium radii is the same, i.e.,  $R_{10} = R_{10} = 8 \mu m$ . As explained in the paragraph following Eq. (19), the strong nonlinear coupling hinders the equality of the radial velocities even when bubbles are of the same size. As shown in Fig. 3(b), both bubbles exhibit nonlinear resonance jump beyond their critical Blake radius of  $35 \mu m$  at 1.3 atm. Interestingly, the jump is not the same for both bubbles. The respective plots from the weak nonlinear coupling are not shown since the curves for the two bubbles then essentially coincide. Further, in light of the linear theory approach from Ref. [26], the resonance frequencies for the symmetric and asymmetric modes of this bubble-system is suppose to be identical. Clearly, the observations from Fig. 3 are against the predictions from the linear theory as well as from the weak nonlinear theory. But, a divergence of the resonance frequencies for closely-spaced identical bubbles has already been described due to radiative coupling by Feuillade [27].

The bubble pair, (8, 8), shown in Fig. 3 yields secondary Bjerknes force,  $\langle F_{12}^s \rangle = +0.17 \mu N$  and  $\langle F_{12}^s \rangle = -0.18 \mu N$ , at  $P_s = 1$  atm, and  $f_s = 30$  kHz. The respective values of the forces at 1.3 atm are,  $-1.33 \mu N$ , and  $-5.1 \mu N$ , respectively. For weak nonlinear coupling,  $\langle F_{12}^w \rangle = \langle F_{21}^w \rangle = -0.07 \mu N$  at  $P_s = 1$  atm, and  $\langle F_{12}^w \rangle = \langle F_{21}^w \rangle = -2.6 \mu N$  at  $P_s = 1.3$  atm. In

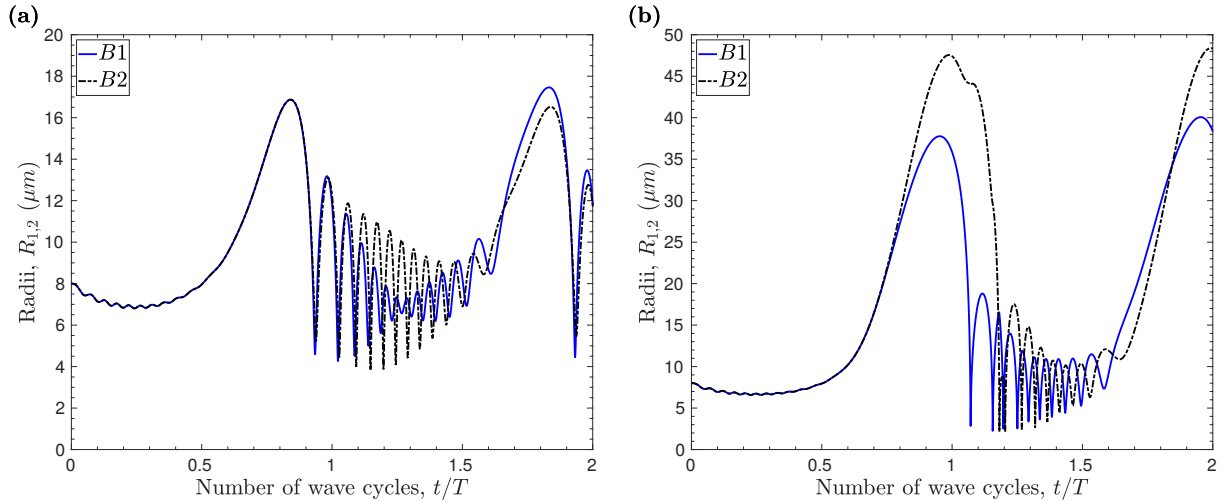


FIG. 3. (Color online) Radii evolution in strong nonlinear coupling for the bubble-pair;  $B_1$  (solid line) and  $B_2$  (dash-dotted line), with  $R_{10} = R_{20} = 8 \mu m$ , separated by a distance of  $128 \mu m$ , for the first two wave cycles of frequency,  $f_s = 30 \text{ kHz}$ . Subfigures (a) and (b) correspond to the conditions,  $P_s = 1 \text{ atm}$ , and  $1.3 \text{ atm}$  respectively.

the case of strong coupling, the same pair when separated by just two times their combined equilibrium radii exerts Bjerknes force of approximately,  $\langle F_{12}^s \rangle = +3.1 \mu N$ , and  $\langle F_{21}^s \rangle = -2 \mu N$ , for all three magnitudes of the driving pressure,  $0.1 \text{ atm}$ ,  $0.05 \text{ atm}$ , and  $0.01 \text{ atm}$ . Thus at such weak driving fields, strong nonlinear coupling predicts a net repulsive force between the bubbles. On the contrary, weak coupling predicts attractive force that are of the order of nano-Newton or less. This is interesting since formation of bubble-grapes has been observed when bubbles separated by distances comparable to their equilibrium sizes are excited by weak acoustic fields as low as  $0.035 \text{ atm}$  [19, 21, 23].

#### IV. CONCLUSION

The implications of strong nonlinear coupling in cavitation bubble-pairs has been investigated. It is found that the bubble-bubble interaction involves two mechanisms. First, the regular radiation coupling between the bubbles. Second, the interaction mediated by the fluid flow that arises predominantly in the near field due to the volume pulsations of the bubbles. The effects of the strong nonlinear coupling is seen in closely-spaced symmetric bubble-pairs as well as in asymmetric bubble-pairs. The results obtained from strong coupling are different compared to those from the weak coupling in weak, regular, and strong acoustic fields. The asymmetry in magnitude as well as in the sign of secondary Bjerknes force is obtained if strong coupling is taken into account. It is envisioned that the strong coupling led sign reversal of the Bjerknes force in a weak acoustic field may play a role in the formation stable bubble clusters. Interestingly, the inherent asymmetric nature of the Bjerk-

nes force may possibly explain why theories motivated from the study of pulsating spheres could not succeed in describing the symmetric laws of gravitation and electromagnetism [12].

Further, the nonlinear resonance jumps observed for smaller bubble in a strong driving field is attributed to the lowering of the dynamical Blake threshold pressure which arises due to the convective fluid flow from the volume pulsations of the bigger bubble. Such nonlinear resonance jumps are observed even in the case of symmetric bubble-pairs, implying bubbles of the same size may not share the same resonance frequency if they are strongly coupled. It is expected that the results reported here may be useful in industrial applications where manipulating bubble-clusters to control cavitation effects is required. A quantitative analysis of the divergence of the resonance frequencies, the lowering of the critical threshold pressure, and the presence of charges, in strongly coupled bubble-pairs is intended for future work.

## ACKNOWLEDGMENT

The derivation part of this study was partly completed during author's postdoctoral stay at the UiT The Arctic University of Norway in Tromsø. Therefore, the author would like to acknowledge the funding provided by Statoil's "Akademia" program, and ARCEX (Research Council of Norway grant number 228107).

- 
- [1] S. Wu, Z. Zuo, H. A. Stone, and S. Liu. Motion of a free-settling spherical particle driven by a laser-induced bubble. *Phys. Rev. Lett.*, 119:084501, 2017.
  - [2] E. Zilonova, M. Solovchuk, and T. W. H. Sheu. Bubble dynamics in viscoelastic soft tissue in high-intensity focal ultrasound thermal therapy. *Ultrason. Sonochem.*, 40:900 – 911, 2018.
  - [3] W. Lauterborn and T. Kurz. Physics of bubble oscillations. *Rep. Prog. Phys.*, 73:106501, 2010.
  - [4] P. Koukouvini, M. Gavaises, O. Supponen, and M. Farhat. Simulation of bubble expansion and collapse in the vicinity of a free surface. *Phys. Fluids*, 28:052103, 2016.
  - [5] C-Y. Lai, J. Eggers, and L. Deike. Bubble bursting: Universal cavity and jet profiles. *Phys. Rev. Lett.*, 121(14):144501, 2018.
  - [6] L. Rayleigh. Viii. on the pressure developed in a liquid during the collapse of a spherical cavity. *Philos. Mag.*, 34(200):94–98, 1917.
  - [7] K. Weinberg and M. Ortiz. Kidney damage in extracorporeal shock wave lithotripsy: a numerical approach for different shock profiles. *Biomech. Model. Mechan.*, 8:285–299, 2009.
  - [8] K. Kooiman, M. Foppen-Harteveld, A. F. W. van der Steen, and N. de Jong. Sonoporation of endothelial cells by vibrating targeted microbubbles. *J. Control. Rel.*, 154(1):35 – 41, 2011.
  - [9] D. Rabaud, P. Thibault, M. Mathieu, and P. Marmottant. Acoustically bound microfluidic bubble crystals. *Phys. Rev. Lett.*, 106:134501, 2011.

- [10] A. O. Maksimov, B. A. Burov, A. S. Salomatin, and D. V. Chernykh. Sounds of marine seeps: A study of bubble activity near a rigid boundary. *J. Acoust. Soc. Am.*, 136(3):1065–1076, 2014.
- [11] B. Verhaagen and D. F. Rivas. Measuring cavitation and its cleaning effect. *Ultrason. Sonochem.*, 29:619–628, 2016.
- [12] L. A. Crum. Bjerknes forces on bubbles in a stationary sound field. *J. Acoust. Soc. Am.*, 57(6):1363–1370, 1975.
- [13] K. Yoshida, T. Fujikawa, and Y. Watanabe. Experimental investigation on reversal of secondary bjerknes force between two bubbles in ultrasonic standing wave. *J. Acoust. Soc. Am.*, 130:135–144, 2011.
- [14] J. Jiao, Y. He, S. E. Kentish, M. Ashokkumar, R. Manasseh, and J. Lee. Experimental and theoretical analysis of secondary bjerknes forces between two bubbles in a standing wave. *Ultrasonics*, 58:35–42, 2015.
- [15] B. Han, K. Köhler, K. Jungnickel, R. Mettin, W. Lauterborn, and A. Vogel. Dynamics of laser-induced bubble pairs. *J. Fluid Mech.*, 771:706–742, 2015.
- [16] T. Barbat, N. Ashgriz, and C.-S. Liu. Dynamics of two interacting bubbles in an acoustic field. *J. Fluid Mech.*, 389:137–168, 1999.
- [17] E. Zabolotskaya. Interaction of gas-bubbles in a sound field. *Sov. Phys. Acoust.*, 30:365–368, 1984.
- [18] H. A. Oguz and A. Prosperetti. A generalization of the impulse and virial theorems with an application to bubble oscillations. *J. Fluid Mech.*, 218:143–162, 1990.
- [19] A. A. Doinikov and S. T. Zavtrak. On the "bubble grapes" induced by a sound field. *J. Acoust. Soc. Am.*, 99:3849–3850, 1995.
- [20] N. A. Pelekasis and J. A. Tsamopoulos. Bjerknes forces between two bubbles. part 2. response to an oscillatory pressure field. *J. Fluid Mech.*, 254:501–527, 1993.
- [21] A. A. Doinikov and S. T. Zavtrak. On the mutual interaction of two gas bubbles in a sound field. *Phys. Fluids*, 7, 1995.
- [22] A. A. Doinikov. Effects of the second harmonic on the secondary bjerknes force. *Phys. Rev. E*, 59:3016, 1999.
- [23] M. Ida. Alternative interpretation of the sign reversal of secondary bjerknes force acting between two pulsating gas bubbles. *Phys. Rev. E*, 67:056617, 2003.
- [24] A. A. Doinikov. Mathematical model for collective bubble dynamics in strong ultrasound fields. *J. Acoust. Soc. Am.*, 116(2):821–827, 2004.
- [25] A. Harkin, T. J. Kaper, and A. Nadim. Coupled pulsation and translation of two gas bubbles in a liquid. *J. Fluid. Mech.*, 445:377–411, 2001.
- [26] M. Lanoy, C. Derec, A. Tourin, and V. Leroy. Manipulating bubbles with secondary bjerknes forces. *Appl. Phys. Lett.*, 107(21):214101, 2015.

- [27] C. Feuillede. Scattering from collective modes of air bubbles in water and the physical mechanism of superresonances. *J. Acoust. Soc. Am.*, 98:1178–1190, 1995.
- [28] N. Sugita and T. Sugiura. Nonlinear normal modes and localization in two bubble oscillators. *Ultrasonics*, 74:174–185, 2017.
- [29] Y. Zhang and Y. Zhang. Chaotic oscillations of gas bubbles under dual-frequency acoustic excitation. *Ultrason. Sonochem.*, 40:151–157, 2018.
- [30] W. Lauterborn and E. Cramer. Subharmonic route to chaos observed in acoustics. *Phys. Rev. Lett.*, 47:1445–1448, 1981.
- [31] W. Lauterborn and U. Parlitz. Methods of chaos physics and their application to acoustics. *J. Acoust. Soc. Am.*, 84(6):1975–1993, 1988.
- [32] O. Louisnard and J. González-García. Acoustic cavitation. In *Ultrasound technologies for food and bioprocessing*, pages 13–64. Springer, 2011.
- [33] S. Behnia, A. J. Sojahrood, W. Soltanpoor, and O. Jahanbakhsh. Towards classification of the bifurcation structure of a spherical cavitation bubble. *Ultrasonics*, 49:605–610, 2009.
- [34] T. Hongray, B. Ashok, and J. Balakrishnan. Oscillatory dynamics of a charged microbubble under ultrasound. *Pramana-J. Phys.*, 84:517–541, 2015.
- [35] T. Hongray, B. Ashok, and J. Balakrishnan. Effect of charge on the dynamics of an acoustically forced bubble. *Nonlinearity*, 27:1157–1179, 2014.
- [36] T. Watanabe and Y. Kukita. Translational and radial motions of a bubble in an acoustic standing wave field. *Phys. Fluids A*, 11:2682–2688, 1993.
- [37] J. Ma, C-T. Hsiao, and G. L. Chahine. Numerical study of acoustically driven bubble cloud dynamics near a rigid wall. *Ultrason. Sonochem.*, 40:944–954, 2018.
- [38] Y. A. Pishchalnikov, J. C. Williams, and J. A. McAteer. Bubble proliferation in the cavitation field of a shock wave lithotripter. *J. Acoust. Soc. Am. Exp. Lett.*, 130(2):EL87–EL93, 2011.
- [39] M. Guédra, C. Cornu, and C. Inserra. A derivation of the stable cavitation threshold accounting for bubble-bubble interactions. *Ultrason. Sonochem.*, 38:168–173, 2017.
- [40] G. L. Chahine. Pressures generated by a bubble cloud collapse. *Chem. Eng. Commun.*, 28:355–367, 1984.
- [41] K. Kooiman, H. J. Vos, M. Versluis, and N. de Jong. Acoustic behavior of microbubbles and implications for drug delivery. *Adv. Drug Deliv. Rev.*, 72:28–48, 2014.
- [42] N. A. Pelekasis and J. A. Tsamopoulos. Bjerknes forces between two bubbles. part 1. response to a step change in pressure. *J. Fluid Mech.*, 254:467–499, 1993.
- [43] Yu. A. Ilinskii and E. A. Zabolotskaya. Cooperative radiation and scattering of acoustic waves by gas bubbles in liquids. *J. Acoust. Soc. Am.*, 92:2837–2841, 1992.
- [44] A. O. Maksimov and V. I. Yusupov. Coupled oscillations of a pair of closely spaced bubbles. *Eur. J. of Mech. B-Fluid*, 60:164–174, 2016.
- [45] G. L. Chahine and R. Duraiswami. Dynamical interactions in a multi-bubble cloud. *J. Fluids Eng.*, 114(4):680–686, December 1992.

- [46] K. Yasui, J. Lee, T. Tuziuti, A. Towata, T. Kozuka, and Y. Iida. Influence of the bubble-bubble interaction on destruction of encapsulated microbubbles under ultrasound. *J. Acoust. Soc. Am.*, 126(3):973–982, 2009.
- [47] J. Glimm, X. L. Li, R. Menikoff, D. H. Sharp, and Q. Zhang. A numerical study of bubble interactions in rayleigh–taylor instability for compressible fluids. *Phys. Fluids A-Fluid*, 2(11):2046–2054, 1990.
- [48] T. J. Matula, R. A. Roy, P. D. Mourad, W. B. McNamara III, and K. S. Suslick. Comparison of multibubble and single-bubble sonoluminescence spectra. *Phys. Rev. Lett.*, 75:2602–2605, 1995.
- [49] S. Hatanaka, K. Yasui, T. Kozuka, T. Tuziuti, and H. Mitome. Influence of bubble clustering on multibubble sonoluminescence. *Ultrasonics*, 40:655–660, 2002.
- [50] Y. T. Didenko and T. V. Gordeychuk. Multibubble sonoluminescence spectra of water which resemble single-bubble sonoluminescence. *Phys. Rev. Lett.*, 84(24):5640, 2000.
- [51] C. Cairós and R. Mettin. Simultaneous high-speed recording of sonoluminescence and bubble dynamics in multibubble fields. *Phys. Rev. Lett.*, 118:064301, 2017.
- [52] M. Ida. Bubble-bubble interaction: A potential source of cavitation noise. *Phys. Rev. E*, 79:016307, 2009.
- [53] K. Yasui, T. Tuziuti, J. Lee, T. Kozuka, A. Towata, and Y. Iida. Numerical simulations of acoustic cavitation noise with the temporal fluctuation in the number of bubbles. *Ultrason. Sonochem.*, 17(2):460–472, 2010.
- [54] J. H. Song, K. Johansen, and P. Prentice. An analysis of the acoustic cavitation noise spectrum: The role of periodic shock waves. *J. Acoust. Soc. Am.*, 140(4):2494–2505, 2016.
- [55] J. Liang, G. Han, L. Fengbin, and C. Darong. Investigations on dynamics of interacting cavitation bubbles in strong acoustic fields. *Ultrason. Sonochem.*, 34:90–97, 2017.
- [56] K. L. de Graaf, I. Penesis, and P. A. Brandner. Modelling of seismic airgun bubble dynamics and pressure field using the gilmore equation with additional damping factors. *Ocean Eng.*, 76:32–39, 2014.
- [57] B. Aktas, M. Atlar, S. Turkmen, W. Shi, R. Sampson, E. Korkut, and P. Fitzsimmons. Propeller cavitation noise investigations of a research vessel using medium size cavitation tunnel tests and full-scale trials. *Ocean Eng.*, 120:122–135, 2016.
- [58] N. Ochiai and J. Ishimoto. Computational study of the dynamics of two interacting bubbles in a megasonic field. *Ultrason. Sonochem.*, 26:351–360, 2015.
- [59] R. Mettin, I. Akhatov, U. Parlitz, C. D. Ohl, and W. Lauterborn. Bjerknes forces between small cavitation bubbles in a strong acoustic field. *Phys. Rev. E*, 56:2924–2931, 1997.
- [60] J. B. Keller and I. I. Kolodner. Damping of underwater explosion bubble oscillations. *J. App. Phys.*, 27(10):1152–1161, 1956.
- [61] A. A. Doinikov. Translational motion of two interacting bubbles in a strong acoustic field. *Phys. Rev. E*, 64:026301, 2001.

- [62] N. A. Pelekasis, A. Gaki, A. Doinikov, and J. A. Tsamopoulos. Secondary Bjerknes forces between two bubbles and the phenomenon of acoustic streamers. *J. Fluid Mech.*, 500:313–347, 2004.
- [63] A. Prosperetti. Free oscillations of drops and bubbles: the initial-value problem. *J. Fluid Mech.*, 100:333–347, 1980.
- [64] A. Prosperetti. Bubble phenomena in sound fields: part one. *Ultrasonics*, 22:69–77, 1984.
- [65] K. E. Chlouverakis and J. C. Sprott. Chaotic hyperjerk systems. *Chaos, Solitons Fract.*, 28(3):739–746, 2006.
- [66] H. Motohashi and T. Suyama. Third order equations of motion and the Ostrogradsky instability. *Phys. Rev. D*, 91:085009, 2015.
- [67] S. M. Cox, D. Schmidt, Y. Modarres-Sadeghi, and S. N. Patek. A physical model of the extreme mantis shrimp strike: kinematics and cavitation of ninkajou. *Bioinspir. Biomim.*, 9(1):016014, 2014.
- [68] X. Huang, Q-X. Wang, A-M. Zhang, and J. Su. Dynamic behaviour of a two-microbubble system under ultrasonic wave excitation. *Ultrason. Sonochem.*, 43:166–174, 2018.
- [69] A. Prosperetti. Bubble dynamics: Some things we did not know ten years ago. In J. R. Blake, J. M. Boulton-Stone, and N. H. Thomas, editors, *Bubble Dynamics and Interface Phenomena*, pages 3–16, 1993.
- [70] A. Harkin, A. Nadim, and T. J. Kaper. On acoustic cavitation of slightly subcritical bubbles. *Phys. Fluids*, 11(2):274–287, 1999.
- [71] M. Ida. Multibubble cavitation inception. *Phys. Fluids*, 21:113302, 2009.